CHAPTER 17

β-Ray Spectra

Among nuclear spectra, that of the β rays has the unique property of being *continuous*. In each β-ray spectrum, there are electrons of all energies up to a definite maximum value. This maximum value is characteristic of the particular radionuclide.

The first 30 years of β-ray spectroscopy were consumed in establishing the general characteristics of the β-ray continuum, as seen in the naturally occurring negatron β-ray emitters, principally RaE.

A successful theory of the shape of β-ray spectra and the lifetime of β-ray emitters was provided by Fermi in 1934, and in the same year a large number of new negatron and positron β-ray emitters became available through the discovery of artificial radioactivity. Progress has been more rapid since then, and by the early 1950s many of the fundamental problems concerning β-ray spectra had been solved. We shall review here the established characteristics of β-ray spectra, in terms of the original discovery experiment when feasible. Further details, including the many experimental and theoretical pitfalls which have repeatedly brought about temporary setbacks, will be found in an abundance of excellent reviews on β decay and β-ray spectroscopy (K39, S43, C8, P32, S37*a*).

1. *Experimental Characteristics of the β-Ray Continuum*

a. Exponential Absorption of the β-Ray Continuum. The absorption curve for β rays displays a characteristic exponential shape. As the absorber thickness is increased, the fractional transmission decreases nearly exponentially but finally drops to zero when the absorber thickness equals the maximum range of the β rays (F12). When these absorption characteristics were first discovered (S13, H4), about 1907, it was known that the absorption curves for γ rays and X rays are exponential. However, the only previously known corpuscular radiation, the α ray, exhibits a definite range and not an exponential absorption curve. Magnetic deflection experiments by W. Wilson, J. A. Gray, and especially by J. Chadwick in 1914 (C10) first showed that the primary spectrum of β rays is continuous and provided a qualitative explanation for the originally puzzling experiments on the absorption and scattering of β rays (R44).

b. Line Spectra of Conversion Electrons. Many β-ray substances emit γ rays also. Therefore their continuous β-ray spectra are accompanied by line spectra of conversion electrons. The relationship between the conversion electrons and γ rays was not recognized until 1922. Prior to that time, the conversion electrons erroneously were thought to be disintegration electrons and possibly to represent the primary spectrum. The line spectrum of conversion electrons was originally called the "line spectrum of β rays," or the "natural β-ray spectrum" (R50). We shall reserve the term β ray for the continuous spectrum of negatrons, or of positrons, emitted by the nucleus.

The conversion electrons are truly associated only with γ decay and can therefore occur whenever γ decay accompanies α decay, β decay, EC transitions, or isomeric transitions. Experimentally, their prominent intrusion in negatron β-ray spectra is an annoying but accidental consequence of the physical identity of atomic electrons and the negatively charged β-ray electrons.

c. Typical β-Ray Spectra. A remarkably wide variety of magnetic focusing β-ray spectrometers has been developed for the accurate measurement of the shape of β-ray spectra. Descriptions of these instruments will be found in a number of review articles (C8, P18) and in the current periodical literature. Because a magnetic filter is a momentum sorting instrument, the experimental results usually are reported as a momentum spectrum, rather than as an energy spectrum. For orientation, Figs. 1.1 to 1.6 show the β-ray spectra of representative, carefully studied nuclides, on both momentum and energy scales.

Note in Fig. 1.1 the asymmetry of the momentum ($B\rho$) distribution of β rays from RaE. This overabundance of low-momentum β rays is characteristic of the spectral shape for many, but not all, *forbidden* transitions. When the spectrum is translated into an energy distribution, as in Fig. 1.2, the asymmetry is especially marked.

Figure 1.3 shows the momentum distribution for the much-studied *negatron* β-ray spectrum of Cu^{64}. Note the high degree of symmetry, which is characteristic of *allowed* β^- spectra. On Gamow-Teller selection rules, as discussed in Chap. 6, both the negatron and the positron β-ray transitions of Cu^{64} are allowed transitions, $p_{\frac{3}{2}} \rightarrow f_{\frac{3}{2}}$, with $\Delta I = 1$, no, (N23). In Fig. 1.4, the corresponding energy distribution is seen to be asymmetric, greatly favoring β rays of small energy. The average β-ray energy is about 0.3 E_{max}(M11).

Figure 1.5 shows the *positron* β-ray momentum distribution of Cu^{64}. This spectrum is also characteristic of allowed transitions. Note especially how the low-momentum end of the positron spectrum differs from the allowed negatron spectrum, as a consequence of the interaction between the β ray and the coulomb potential of the nucleus. Positrons with very low momentum are scarce in the spectrum, and the most probable momentum is slightly greater than one-half the maximum momentum. In the corresponding positron energy distribution, Fig. 1.6, the usual asymmetry is seen. The average β-ray energy is about 0.4 E_{max} (M11). In common with all β-ray energy distributions, there is a definite

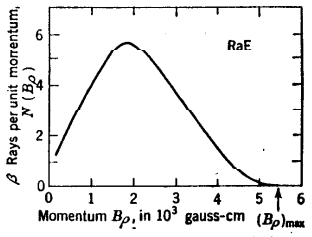

Fig. 1.1 Momentum spectrum of the β rays from RaE, a forbidden transition. [*From Neary* (N7).]

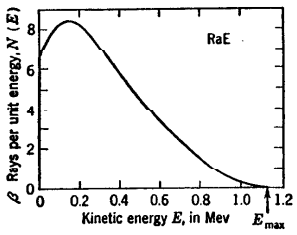

Fig. 1.2 Energy spectrum of the β rays from RaE. [*From Neary* (N7).]

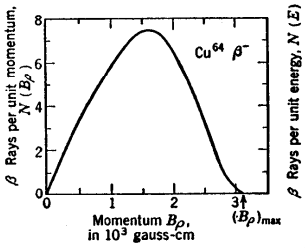

Fig. 1.3 Momentum spectrum of the negatron β rays from Cu^{64}, an allowed transition. [*From Reitz* (R14).]

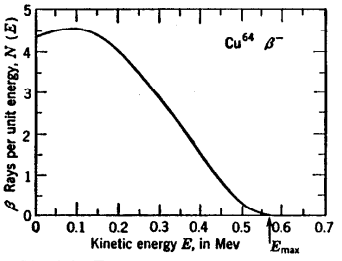

Fig. 1.4 Energy spectrum of the negatron β rays from Cu^{64}. (Calculated from Fig. 1.3.)

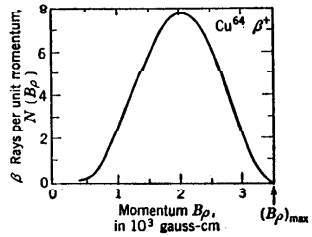

Fig. 1.5 Momentum spectrum of the positron β rays from Cu^{64}, an allowed transition. [*From Reitz* (R14).]

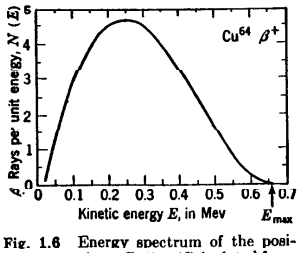

Fig. 1.6 Energy spectrum of the positron β rays from Cu^{64}. (Calculated from Fig. 1.5.)

upper limit, at an energy E_{max}. Near this upper limit, the number-energy distribution approaches the energy axis as a "second-order contact," i.e., the number of β rays in successive energy intervals, E to $E + dE$, decreases approximately as the square of $(E_{max} - E)$.

d. Change in Nuclear Charge Accompanying β Decay. The very early radiochemical work by Soddy, Boltwood, and others showed that β decay is accompanied by a shift in chemical properties and corresponds to a change of one unit in atomic number. This principle became part of Soddy's displacement law (Chap. 1, Sec. 5) and was easily demonstrated among the β emitters of the naturally occurring radioactive series because both parent and product are often radioactive, as in the case of $_{83}RaE^{210} \xrightarrow{\beta^-} {}_{84}Po^{210} \xrightarrow{\alpha} {}_{82}Pb^{206}$. For positron β-ray emitters, such as $_{11}Na^{22} \xrightarrow{\beta^+} {}_{10}Ne^{22}$, the stable decay product has not been accumulated in chemically manageable quantities. Nevertheless, the atomic number of the decay product can be determined unambiguously by means of the energy separation of the conversion electrons. It is therefore certain that the disintegration β rays comprise a *primary* spectrum. In particular, the continuous negatron β-ray spectrum is not a secondary spectrum of accelerated atomic electrons, produced by some as yet undiscovered process.

e. Number of β Rays per Disintegration. Direct physical measurements of the total number of negatrons emitted by β-ray bodies which are in radioactive equilibrium with an α-ray substance whose disintegrations can be counted readily, such as $RaE \xrightarrow{\beta^-} Po \xrightarrow{\alpha} Pb$ (E13), invariably show that *one β ray is emitted by each disintegrating atom.* Conversion electrons, if present, will, of course, augment the total number of negatrons emitted. Thus ThB emits a total of about 1.4 electrons per disintegration (R50), but 0.4 of these are atomic electrons ejected by internal conversion of the excited product nucleus.

f. Average Energy of β Rays. We have seen that α rays are emitted from nuclei as monoenergetic groups. Thus the energy difference between parent and product is the same for all nuclei in the group, and all nuclei of a given type are energetically identical. If all RaE nuclei are identical, and all their decay product nuclei (polonium) are identical, the law of conservation of energy requires that the same amount of energy be emitted in every β-ray disintegration of RaE. It was therefore proposed that all β rays are ejected from the nucleus with the same energy, corresponding to the maximum energy of continuous spectrum, but that while emerging through the cloud of atomic electrons some absorption or other degradation process intervened to produce a continuous spectrum. If this were the case, the average energy of disintegration as measured in a calorimeter would equal E_{max}, because any kinetic energy imparted to the atomic electrons must eventually appear as heat.

In order to determine whether or not the observed continuous spectrum is the primary spectrum, microcalorimeter measurements were first made on RaE in 1927. The number of disintegrations involved and the calibration constant of the calorimeter can be obtained by subsequent observations on the α rays from polonium, the decay product of RaE.

For RaE, $E_{max} = 1.17$ Mev. Microcalorimeter observations by Ellis and Wooster (E11) gave 0.35 ± 0.04 Mev for the average energy of disintegration. The experiment was improved and repeated by Meitner and Orthmann (M40) who obtained 0.34 ± 0.02 Mev and by Zlotowski (Z2) who found 0.320 ± 0.005 Mev. These measurements provide complete confirmation of the results of this fundamental experiment and show that for RaE the average energy of the disintegration β rays is only $(0.28 \pm 0.01)\ E_{max}$. This value is in agreement with the mean energy deduced from the observed β-ray spectrum, seen in Fig. 1.2. These findings have been amply confirmed by microcalorimeter measurements on simple β-ray emitters (M76) such as $P^{32}(E_{max} = 1.70$ Mev) which emits 4.15 μw/mc (Z4) and thus has an average energy of 0.70 Mev, or $0.41\ E_{max}$, in agreement with its measured β-ray spectral distribution. It must be concluded that *the observed continuous spectrum portrays the primary distribution of β-ray energies as emitted by the disintegrating nucleus.*

g. Decay Constant in Various Portions of the β-Ray Spectrum. Many observations have been made on the radioactive decay constant of β rays in various portions of the continuous spectrum. Invariably, *the rate of decay is independent of the portion of the β-ray spectrum which is chosen.* This is equivalent to saying that the shape of the β-ray spectrum does not vary with the age of a given sample of a radionuclide. (Routine tests for contamination in β-ray sources are based on this well-established principle.) Physically, this observation means that all the nuclei in a given radionuclide are identical and that each nucleus has a partial decay constant, say, λ_E, for disintegrating with a β-ray energy between E and $E + dE$. The sum of these partial decay constants, from $E = 0$ to $E = E_{max}$, is the total probability of decay λ for each nucleus. The residual stock of untransformed nuclei then decreases as $e^{-\lambda t}$, and the activity in any energy band E to $E + dE$ decreases at the same rate.

h. Decay Energy Equals the Maximum Energy of the β-Ray Spectrum. Sargent showed in 1933 that nuclides which have large values of the upper limit of their β spectrum also have large decay constants (Fig. 3.1, Chap. 6). With this and other evidence in view, Ellis and Mott (E10) proposed that the energy difference between the parent and product nuclei equals the upper limit E_{max} of the β spectrum. This interpretation has proved to be entirely correct (Chap. 3, Sec. 4) but in 1933 it was a bold assumption, concerning which Ellis and Mott remarked:

> We do not wish in this paper to dwell on what happens to the excess energy in those disintegrations in which the electron is emitted with less than the maximum energy. We may, however, point out that if the energy merely disappears, implying a breakdown of the principle of energy conservation, then in a β-ray decay energy is not even statistically conserved. Our hypothesis is, of course, also consistent with the suggestion of Pauli that the excess energy is carried off by particles of great penetrating power such as neutrons of electronic mass.

The first good experimental proof that E_{max} equals the disintegration energy in β^- decay was the observation by W. J. Henderson (H36) that the total energy of the branch disintegration of ThC into ThD is the same

for the two branches ${}_{83}\text{ThC} \xrightarrow{\beta} {}_{84}\text{ThC}' \rightarrow {}_{82}\text{ThD}$, and ${}_{83}\text{ThC} \rightarrow {}_{81}\text{ThC}'' \xrightarrow{\beta} {}_{82}\text{ThD}$, provided that the two β transformations are represented by the maximum energy of their respective β-ray spectra. The decay schemes and the energetics of these branch transformations are shown in Fig. 1.3 of Chap. 16. This proof involves the difference between two β-ray spectra, and the later measurements on individual artificially radioactive nuclides are even more compelling (e.g., Chap. 3, Sec. 4, Prob. 8).

2. *The Neutrino*

The neutral particle of great penetrating power which Pauli (P8) proposed informally about 1931 is now well established as a consequence of extensive experimental and theoretical work. Fermi's theory of β decay, in 1934, developed for the first time a set of measurable consequences of the existence of a neutrino, and these have now been completely verified experimentally. Before discussing the details of Fermi's theory of β decay, we may survey briefly the principal experimental evidence concerning the neutrino.

a. Conservation Laws. In the beginning, we may regard the neutrino as a particle whose properties are selected in such a way that β decay can take place without violating any of the conservation laws. Each β disintegration is to involve the simultaneous emission of one β-ray electron and one neutrino.

Charge is already conserved by the disintegration electron in β decay; hence the neutrino has *zero charge*. The energetics of light-element reactions (L27) shows that the mass-energy balance in β decay is exact, within an experimental uncertainty of about 4 kev, when the kinetic energy of the residual atom and of the β rays of maximum energy E_{max} is considered. Therefore the neutrinos which accompany these β rays can have a rest mass which is at most 1 per cent that of an electron and is probably identically zero. We shall see later that the rest mass of the neutrino also influences the shape of the β-ray spectrum near E_{max}, and that theory and experiment are in accord with *zero rest mass* for the neutrino.

In β decay, the parent and product nuclei always have the same mass number. This requires (Chap. 4, Sec. 7) that both have the same statistics and that their nuclear angular momenta may differ only by zero or an integer multiple of $\hbar$. But the β-ray electron has Fermi-Dirac statistics and a spin of $\hbar/2$. In order to conserve statistics and angular momentum, the neutrino must also have *Fermi-Dirac statistics* and an *intrinsic spin of $\hbar/2$*.

A neutrino of zero charge and zero rest mass could be expected (B40) to ionize air only to the minute extent of $10^{-8}\ \mu^2$ ion pairs per centimeter of path, where μ is its magnetic dipole moment in Bohr magnetons. The neutrinos are not absorbed by small thicknesses of material, as is shown by the fact that they produce no effect in a β-ray calorimeter. Nahmias (N2) filtered the α, β, and γ rays emitted by 5 g of radium, with up to 91

cm of Pb, and showed that residual ionization by neutrinos was not detectable. This corresponds to an ionization mean free path which exceeds 10^6 g/cm^2, and it also places an upper limit of about 1/4,000 Bohr magneton, or one-half nuclear magneton, on the *magnetic moment*, if any, of the neutrino. Nahmias's negative result shows that the cross section for interaction of a neutrino with an electron is smaller than 10^{-21} cm^2 (10^{-7} barn) per electron. Cowan et al. (C47*a*) deduce an upper limit of 10^{-7} Bohr magneton for the magnetic moment of the neutrino, based on observations of a liquid scintillator irradiated by neutrinos from a fission reactor. Wollan (W68) showed that the cross section for interaction of a neutrino with a proton is smaller than 2×10^{-30} cm^2 because the intense flux of neutrinos outside the shield of a uranium reactor produces no detectable ionization in a hydrogen-filled chamber. The neutrino indeed fulfills Pauli's specification of great penetrating power.

b. Neutrino Recoil Measurements. Any β ray whose kinetic energy is E must be accompanied by a neutrino whose kinetic energy is

$$E_\nu = (E_{max} - E)$$

From relativistic dynamics (Appendix D), any particle with zero rest mass can carry kinetic energy only if it has the *velocity of light c*. The *momentum* p_ν of the neutrino is then $p_\nu = E_\nu/c = (E_{max} - E)/c$. For kinetic energies which are appreciably greater than $m_0c^2 = 0.51$ Mev, neutrinos and β rays will have comparable momenta. It is therefore feasible to study experimentally the momentum relationships in β decay. A number of such experiments have been conducted successfully, and the methods and results up to 1948 were admirably reviewed by Crane (C50), by Allen (A15), and by Gamow (G6).

The experimental approach involves a measurement of the momentum relationships between the β ray and the recoil atom. This can be performed in many ways, the simplest being a measurement of the momentum of the recoil atoms. In the more complete types of experiment, individual disintegrations are studied by coincidence methods and evaluations are obtained for at least two of the three measurable parameters: (1) the momentum of the β ray, (2) the momentum of its own recoil atom, and (3) the angle between the direction of emission of the β ray and the direction of the recoil atom.

In all cases, it is found that linear momentum is not conserved between the β ray and the recoil atom alone. The magnitude and direction of the "missing" momentum are just what would be expected if a neutrino of zero rest mass and energy $(E_{max} - E)$ were involved as a third particle in the disintegration. For example, Sherwin (S34) has measured the momentum of β rays from P^{32} by magnetic deflection, while simultaneously observing the velocity of the recoil atom in a predetermined direction by means of a time-of-flight measurement. In the individual disintegrations, it is found that the missing energy $(E_{max} - E)$ and the missing momentum have the ratio c (± 20 per cent), as is predicted by the conservation laws if the unobserved energy and momentum are to be ascribed to a single "package," the zero-mass neutrino.

Angular Correlation between Neutrino and Electron in β Decay. Analogous measurements have been carried out by Allen and others (A16, R41) on the β rays and the recoil Li^6 atoms produced in the β decay of He^6 ($E_{max} = 3.5$ Mev). Beyond merely confirming the neutrino hypothesis, these experiments begin to furnish good data on the angular correlation between the direction of emission of the neutrino and the β ray.

It can be shown theoretically that the angle ϑ between the direction of emission of the neutrino and the β ray is very sensitive to the fundamental interaction assumed between the transforming nucleon and the electron-neutrino field. For allowed transitions, in nuclides having low atomic number and high-energy β rays, Hamilton (H13) has shown that the neutrino-electron angular correlation function $w(\vartheta)$ has the values given in Table 2.1 for the five possible invariant forms of β interaction, where $\beta \equiv V/c$ is the velocity of the β ray in terms of the velocity of light and $w(\vartheta)$ is the relative probability per unit solid angle that the neutrino will be emitted at an angle between ϑ and $\vartheta + d\vartheta$ with respect to the direction of the β-ray electron.

TABLE 2.1. NEUTRINO-β ANGULAR CORRELATION

ν-β angular correlation function	Form of β interaction	Selection rules
$w(\vartheta) = 1 + (\beta/3)\cos\vartheta$	Tensor	$\Delta I = 0, \pm 1$, no; not $0 \rightarrow 0$
$w(\vartheta) = 1 - (\beta/3)\cos\vartheta$	Axial vector	(Gamow-Teller)
$w(\vartheta) = 1 - \beta\cos\vartheta$	Scalar	$\Delta I = 0$, no (Fermi)
$w(\vartheta) = 1 + \beta\cos\vartheta$	Polar vector	
$w(\vartheta) = 1 - \beta\cos\vartheta$	Pseudoscalar	$\Delta I = 0$, yes

The shape of the β spectrum for allowed transitions is the same for all five possible forms of interaction, but the correct form of interaction can be selected eventually on a basis of ν-β angular-correlation measurements. These experiments are difficult and will require further work before the results become unequivocal. For the interesting He^6 β-ray spectrum ($E_{max} = 3.5$ Mev, $T_{\frac{1}{2}} = 0.8$ sec; $\Delta I = 1$, no; G-T allowed) the ν-β angular-correlation measurements by J. S. Allen and others (A15*a*) are in good agreement with the $1 - (\beta/3)\cos\vartheta$ distribution which characterizes the axial vector interaction. Recoil measurements on A^{35} suggest that the Fermi part of the β interaction may be entirely polar vector.

ν-β Angular Correlation in Forbidden Transitions. In forbidden β transitions, the orbital angular momentum of the transforming nucleon usually changes by one or more units of $\hbar$. This angular momentum must be provided by the emitted neutrino and β ray. Near the middle of the β-ray energy distribution the electron and neutrino have comparable linear momenta, and they tend to be emitted in the same direction (small ϑ), thus utilizing their combined linear momenta to provide the needed nuclear-angular-momentum change. Near the upper energy

limit of the β-ray spectrum the neutrino has a small momentum, while near the lower limit the electron has a small momentum. Parallelism of the neutrino and electron is therefore less important near the two ends of the β-ray energy distribution. But near the middle of the spectrum, *the neutrino and electron tend to be emitted in the same direction in forbidden β-ray transitions.* These qualitative inferences are in agreement with the somewhat complicated analytical expressions of $w(\vartheta)$ for forbidden transitions (H13).

Neutrino Momentum in Electron-capture Transitions. Electron-capture transitions provide the simplest demonstration of neutrino momentum. Following capture by the nucleus of one of its own atomic electrons, the energy of the transition is presumed to be shared between only two bodies, the emitted neutrino and the residual recoil atom. Therefore the spectra of neutrino and of recoil energies should both be monoenergetic, rather than being continuous as in the three-body, β-decay system.

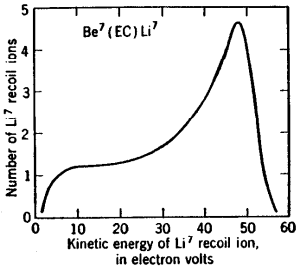

Fig. 2.1 Spectrum of Li^7 recoil energies following electron-capture transitions in Be^7. [*From Davis* (D10).]

When the electron-capture transition goes to the ground level of the decay product there is no complication introduced by recoil from γ-ray emission. Then, from conservation of energy and linear momentum, a recoil atom of mass M should acquire a recoil kinetic energy E_R, from a zero-mass neutrino, given by

$$E_R = \frac{Q^2}{2Mc^2} \qquad (2.1)$$

where Q is the total disintegration energy shared by the neutrino and the recoil atom. In selecting radionuclides for an experimental test of Eq. (2.1), one seeks, among other properties, a large Q and a small mass in order to maximize the available recoil energy. At the same time, Q must be less than 1.02 Mev, in order to exclude positron emission in competition with electron capture.

Two radionuclides which are reasonably satisfactory are Be^7 and A^{37}. The decay scheme of Be^7 is shown in Fig. 4.4 of Chap. 3. About 89 per cent of the EC transitions go to the ground level of Li^7, with $Q = 0.86$ Mev. From Eq. (2.1) these should produce monoenergetic Li^7 recoil atoms having $E_R = 57$ ev, if only one neutrino is emitted per disintegration. Figure 2.1 shows the recoil-energy spectrum as measured by Davis (D10), using a 90° electrostatic analyzer to determine the kinetic energy of singly charged Li^7 ions, which were projected by neutrino recoil from an approximate monolayer of Be^7 deposited on a hot tungsten ribbon. The high-energy peak in Fig. 2.1 has a measured maximum energy of 56 ± 1 ev. The low-energy tail arises in part from the unknown binding energy of Li ions to the tungsten surface and in part

from the continuum of recoil energies which are produced in about 11 per cent of the disintegrations of Be^7, where a 0.38-Mev neutrino emission leads to an excited level in Li^7. This level has a mean life of about 0.8×10^{-12} sec (E0) and a 0.48-Mev γ ray is emitted. Vectorial combination of the momentum from the 0.38-Mev neutrino and the 0.48-Mev γ ray gives a continuous distribution of recoil energies, up to 57 ev. The observed recoil spectrum is consistent with the assumption that one neutrino, having small or zero rest mass, is emitted in each electron-capture disintegration of Be^7.

Although its recoil ions are much heavier, A^{37} has the advantage of being a gaseous source and thus of eliminating uncertainties due to surface work functions. Also, all A^{37} transitions go directly to the ground

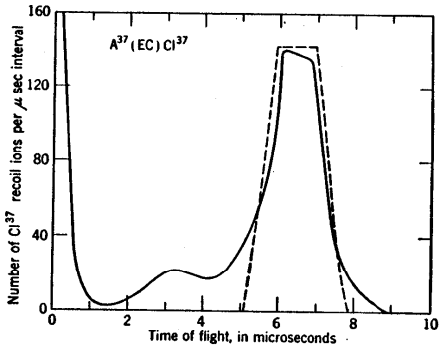

Fig. 2.2 Spectrum of Cl^{37} recoil velocities, as time of flight for a 6-cm path, following electron-capture transitions in A^{37}. The dashed curve is the distribution expected for 9.7-ev monoenergetic recoil ions. [*From Rodeback and Allen* (R23).]

level of its decay product Cl^{37}. There is no interference from γ rays nor β^+ decay. The disintegration energy is $Q = 0.82$ Mev, so that the Cl^{37} recoil energy should be 9.7 ev. Auger electrons are emitted following about 82 per cent of the EC transitions (93 per cent K capture, 7 per cent L capture), but these have energies of about 2.4 kv and do not change the momentum of the recoil atom by more than about 0.2 per cent. Figure 2.2 shows the spectrum of Cl^{37} recoil energies, observed by Rodeback and Allen (R23) using a time-of-flight measurement, the 20-channel timing circuits being triggered by detection of the Auger electron. The maximum distance traveled by the recoil ions is 6.0 cm, and so the time-of-flight measurements correspond to a recoil velocity of (0.71 ± 0.06) cm/μsec, or an energy of 9.7 ± 0.8 ev. In Fig. 2.2, the counts below about 4 μsec are fictitious coincidences caused mostly by scattered Auger electrons. The over-all results are again consistent with the hypothesis that

one neutrino, of zero rest mass, is emitted in each electron-capture transition.

c. Capture of Neutrinos. For all fundamental particles except the neutrino, good experimental data are available on both the "birth" and "death" of the particle, i.e., on its production and on its interactions with matter. The birth and the existence of neutrinos are clear, from the β-ray and electron-capture recoil experiments. Detection of the interactions of free neutrinos with matter has presented a more formidable experimental obstacle.

The only interaction which can be confidently expected is *inverse electron capture*. Here the neutrino would be captured by a nuclear proton or neutron, and a positive or negative electron would be emitted, thus providing for conservation of charge, mass energy, spin, and statistics. These inverse-electron-capture processes can be written

$$p + \bar{\nu} \rightarrow e^+ + n \tag{2.2}$$

and

$$n + \nu \rightarrow e^- + p \tag{2.3}$$

If a distinction exists between neutrinos, ν, and antineutrinos, $\bar{\nu}$, as in Eq. (3.3) of Chap. 8, then Eq. (2.2) represents antineutrino capture and Eq. (2.3) represents neutrino capture.

To test the $n(\nu,e^-)p$ reaction it would be necessary to use neutrons which are bound in nuclei. For an experimental test of the $p(\bar{\nu},e^+)n$ reaction, Crane (C49) chose the reaction

$$_{17}Cl^{35} + \bar{\nu} \rightarrow e^+ + {}_{16}S^{35} \tag{2.4}$$

for study because any S^{35} produced could be isolated chemically and detected by its subsequent β disintegration

$$S^{35} \rightarrow \beta^- + \bar{\nu} + Cl^{35} \tag{2.5}$$

The reactions, Eqs. (2.4) and (2.5), form a cycle in which nothing is accomplished except that the energy of the incident neutrino produces a positron-negatron pair. The threshold energy for the incident neutrino is therefore E_{max} of the β spectrum (0.167 Mev for S^{35}) plus $2m_0c^2$, or $\sim$1.2 Mev. To test the reaction $Cl^{35}(\bar{\nu},e^+)S^{35}$, Crane left a 1-mc source of mesothorium, in equilibrium with its decay products, in the center of a 2 lb bag of NaCl for 90 days (about one half-period for S^{35}). The salt was then dissolved and the sulfur extracted. The absence of detectable β activity in this sulfur fixed the cross section of the $Cl^{35}(\bar{\nu},e^+)S^{35}$ as less than 10^{-30} cm^2, that is, $\sigma < 10^{-6}$ barn.

Theoretical estimates (B48, B43, R13, F41) of σ for the $(\bar{\nu},e^+)$ and (ν,e^-) reactions, with 1- to 2-Mev neutrinos, lead to values of the order of 10^{-42} to 10^{-44} cm^2. These estimates should be reasonably accurate because their basis is essentially the product of the geometrical area $\sim 10^{-24}$ cm^2 of the nucleus and an intrinsic probability of $\sim 10^{-20}$ which is based in principle on the measured half-periods of known electron capture disintegrations. The physical significance of a nuclear cross section of

only 10^{-43} cm^2 is fantastic. Such particles would pass through the sun with very little chance of collision. The thickness of Pb required to attenuate neutrinos by the factor $1/e \simeq 0.37$ is about 10^{20} cm, or 100 light-years of Pb!

A determined and ambitious effort to detect the $(\bar{\nu},e^+)$ capture reaction has been in progress for some time at the Los Alamos Scientific Laboratory and the Hanford Engineering Works. This experiment seems to be succeeding. It undertakes to observe the $(\bar{\nu},e^+)$ reaction on hydrogen, i.e.,

$$H^1 + \bar{\nu} \rightarrow e^+ + n \tag{2.6}$$

by utilizing the intense neutrino flux near the face of a Hanford reactor operating at full power. The hydrogen-containing target consists of about 10 ft^3 of a liquid scintillator material. This large scintillator is viewed by 90 photomultiplier tubes, whose outputs feed an 18-channel time-delay analyzer, with 0.5-μsec channel widths. A time-delayed coincidence is initiated by the appearance and annihilation of a positron in the scintillator. The neutron which is produced at this time undergoes several elastic collisions while being reduced in energy until it is captured in an (n,γ) reaction on Cd ($E_0 = 0.176$ ev, Fig. Introduction.1, Chap. 14) which is present as a salt dissolved in the scintillator. The time-delayed coincidence is terminated by detection of a secondary electron produced by absorption of this capture γ ray in the scintillator.

The energy spectrum of neutrinos emitted in the β decay of fission fragments has been estimated by Alvarez, and from this an effective cross section of about 6×10^{-20} barn is expected for the $H^1(\bar{\nu},e^+)n$ reaction, which has a threshold energy of 1.80 Mev. With this cross section, the available neutrino flux should give a counting rate of about 0.2 count per minute in the scintillator used in 1953. The observed counting rate (R13) was 0.41 ± 0.20 delayed coincidence count per minute. Further work is in progress to improve this measurement. In the meantime, it appears probable that an interaction between free neutrinos and matter has at last been observed.

Problems

1. $_{36}Kr^{88}$ has a half-period of about 3 hr and decays to $_{37}Rb^{88}$ with the emission of β rays having a maximum energy of 2.4 Mev. No important γ rays have been reported. A particular β ray from Kr^{88} is observed to have a radius of curvature of 6.10 cm in a magnetic field of 1,000 gauss.

(*a*) What is the energy, in Mev, of this β ray and of its associated neutrino?

(*b*) What is the kinetic energy of the recoil Rb^{88}, if the angle ϑ between the directions of emission of the β ray and of the neutrino is zero?

(*c*) What is the maximum possible kinetic energy in ev of the recoil from this β-ray disintegration? (Jacobsen observed 51.5 ± 2 ev.)

2. What is the most probable angle ϑ between the electron and neutrino directions in an allowed β-ray transition (*a*) if the β interaction is axial vector with Gamow-Teller selection rules, and (*b*) if the β interaction is polar vector, with Fermi selection rules? *Ans.*: (*a*) $\vartheta \simeq 106°$ for $\beta \rightarrow 1$; (*b*) $\vartheta \simeq 60°$ for $\beta \rightarrow 1$.

3. *Fermi Theory of β Decay*

After the discovery of the neutron in 1932 it became clear that the then known instances of β^- decay were essentially processes in which one neutron in the nucleus transforms into a proton. In 1934 Fermi utilized Pauli's neutrino hypothesis in the first successful quantitative theory of the shape of β^- spectra and of the lifetime of β^--ray emitters. The subsequent discovery of artificial radioactivity brought to light a number of positron emitters. Their β^+ spectra are correctly described by Fermi's original formulation for β^- decay, provided that the nuclear charge Z of the decay product is taken as negative $(-Z)$ for the case of β^+ decay, while remaining positive for β^- decay.

Negatron and positron β decay can then be represented as the transformation of one nucleon in the nucleus, according to

$$n \rightarrow p + \beta^- + \bar{\nu} \tag{3.1}$$

$$p \rightarrow n + \beta^+ + \nu \tag{3.2}$$

where β^- is the ordinary negative electron β ray and β^+ is a positron β ray or, on Dirac's electron theory, a "hole" in the otherwise filled sea of negative energy states for electrons. In a similar way, ν represents the neutrino and $\bar{\nu}$ is the Dirac antineutrino, or "hole" in the negative energy states of neutrinos. The distinction between neutrinos and antineutrinos is significant for the case of double β decay (Chap. 8). For ordinary β decay, as represented by Eqs. (3.1) and (3.2), the physical distinction between $\bar{\nu}$ and ν does not affect the spectral shape, and we shall often refer to either as a neutrino.

The detailed mechanism which underlies Eqs. (3.1) and (3.2) awaits experimental and theoretical clarification. Meson theories of β decay presume that these are two-step processes, involving the formation of a meson which decays into the electron and neutrino pair, but so far these theories have not been successful quantitatively. At present no connection between β decay and the specifically nuclear forces between nucleons has been established.

a. Shape of the Allowed β-Ray Spectrum. In Fermi's theory of β decay (F34, F41, K37, B68, W73) the probability $N(p)\,dp$ that a β ray with momentum between p and $p + dp$ will be emitted in unit time can be written as

$$N(p)\,dp = \frac{2\pi}{\hbar}\,|\psi_e(0)|\,|\psi_\nu(0)|\,|P|g|^2\,\frac{dn}{dE_0} \quad \text{sec}^{-1} \tag{3.3}$$

Here the electron and neutrino, which are created at the moment of emission, are represented as plane waves and have expectation values $|\psi_e(0)|^2$ and $|\psi_\nu(0)|^2$ at the position of the nucleus. The behavior of the transforming nucleon is represented by the transition matrix element $P = \int \psi^*_{\text{initial}} O \psi_{\text{final}}\,d\tau$, where O represents an operator which is appropriate to one of the five possible forms of interaction: scalar, polar vector, tensor, axial vector, or pseudoscalar (K41). The squared modulus $|P|^2$ of the transition matrix element can be interpreted physically as the degree of overlap of the nucleon wave functions for the initial and final states. For allowed transitions, $|P|^2$ is then of the order of unity. In Eq. (3.3), g is a new natural constant, the so-called *Fermi constant*, whose numerical value is determined empirically and is $g \sim 10^{-49}$ cm^3 erg, Eq. (3.34*a*). The characteristic bell shape of the β-ray momentum spectrum is determined primarily by the so-called *statistical factor* dn/dE_0. We shall examine in more detail the statistical factor and the influence of the nuclear charge on the electron function $|\psi_e(0)|^2$.

Statistical Factor. Because of its very large mass, the residual atom receives only a negligible fraction of the kinetic energy in the β disintegration, and so, to a good approximation, kinetic energy is essentially conserved between the neutrino and the β ray. Then if E is the kinetic energy of the β ray and E_0 is the kinetic energy of transformation (the same as $E_{\max}$), the kinetic energy of the neutrino can be written as $(E_0 - E)$ and the momentum of the neutrino as $(E_0 - E)/c$ if its rest mass is zero.

In the β disintegration, momentum is conserved in the three-body system of residual atom, neutrino, and β ray. Because of the presence of the nucleus, momentum need not be conserved between the neutrino and the β ray. Then a β ray whose momentum is p will be associated with a neutrino whose magnitude of momentum q is determined by energy conservation, not momentum conservation, thus

$$p = \frac{1}{c}\sqrt{E(E + 2m_0c^2)} \qquad q = \frac{1}{c}(E_0 - E) \tag{3.4}$$

The statistical distribution of electron momenta in the β-ray spectrum is obtained by considering the volume in phase space which is accessible to an electron whose momentum is between p and $p + dp$ and to an associated neutrino whose momentum is between q and $q + dq$.

The number of electron states in the volume element $4\pi p^2\,dp$ of phase space is

$$2\left(\frac{4\pi p^2\,dp}{h^3}\right) \tag{3.5}$$

and the number of neutrino states, with neutrino momentum between q and $q + dq$, is

$$\frac{4\pi q^2\,dq}{h^3}\Big) \tag{3.6}$$

The momenta p and q are related only through conservation of energy, that is, $q = (E_0 - E)/c$. Then the neutrino momentum interval dq is to be taken per unit range of total energy, while the β-ray energy and momentum are held constant (B68); thus $dq = dE_0/c$. Assembling these factors, we find that the number of accessible final states dn/dE_0 per

unit range of total energy release is

$$\frac{dn}{dE_0} = \frac{4\pi p^2\,dp}{h^3}\frac{4\pi q^2\,dq}{h^3}\frac{1}{dE_0} = \frac{4\pi p^2\,dp}{h^3}\frac{4\pi}{h^3}\frac{(E_0 - E)^2}{c^3}$$
$$= \frac{16\pi^2}{h^6c^3}\,p^2(E_0 - E)^2\,dp \tag{3.7}$$

which is the relative probability that the β-ray momentum will be between p and $p + dp$.

It is convenient to express β-ray momenta and energies as the dimensionless quantities η and W, where

$$\eta \equiv \frac{p}{m_0c} = \frac{mV}{m_0c} = \frac{B\rho(\text{gauss-cm})}{1{,}704} \tag{3.8}$$

$$W \equiv \frac{m}{m_0} = \frac{E + m_0c^2}{m_0c^2} = \frac{E(\text{Mev})}{0.51} + 1 \tag{3.9}$$

The relativistic relationship between the momentum η and the *total* energy W (including the rest energy m_0c^2) then becomes (see Appendix D for details)

$$W^2 = \eta^2 + 1 \tag{3.10}$$

and the electron's velocity V, in terms of the velocity of light c, is simply

$$\beta \equiv \frac{V}{c} = \frac{\eta}{W} \tag{3.11}$$

In terms of η and W, Eq. (3.7) takes on its common form

$$\frac{dn}{dE_0} = \left(\frac{16\pi^2m_0^5c^4}{h^6}\right)\eta^2(W_0 - W)^2\,d\eta \tag{3.12}$$

The statistical factor $\eta^2(W_0 - W)^2\,d\eta$ gives an excellent representation of the shape of allowed β-ray spectra in low-Z nuclides, as represented by the $Z = 0$ curve in Fig. 3.1. For small η, the number of β rays $N(\eta)$ per momentum interval varies approximately as η^2. This parabolic variation is mirrored at the high-energy end of the momentum spectrum, where $N(\eta)$ varies about as $(W_0 - W)^2$, which can be shown to be approximately proportional to $(\eta_0 - \eta)^2$ near the high-energy limit.

Nuclear Coulomb Factor. The emitted β ray experiences a coulomb force while it is in the vicinity of the nucleus. Classically, a negatron β ray would be decelerated by the positively charged nucleus, so that the final spectrum should contain more very slow β^- rays than is given by the statistical factor alone. Conversely, positron β rays would be accelerated, and the final β^+ spectrum should be impoverished in very slow β^+ rays. Qualitatively, β^- and β^+ spectra do differ in just this fashion, as is evident in Figs. 1.3 and 1.5.

Quantitatively, the effect of the nuclear coulomb potential can be evaluated as a perturbation on the electron wave function ψ_e, in Eq. (3.3). The resulting changes in spectral shape are most important in the low-energy end of the β spectrum. A nonrelativistic calculation shows that

the probability $N(\eta)$ of emission of a β ray with momentum between η and $\eta + d\eta$ is altered by the factor

$$F_N(Z,\eta) \sim \frac{2\pi y}{1 - e^{-2\pi y}} \qquad \text{nonrelativistic} \tag{3.13}$$

where

$$y \equiv \frac{\pm Z}{137\beta} = \pm Z\alpha\frac{W}{\eta} \qquad \begin{cases} +Z \text{ for } \beta^- \text{ decay} \\ -Z \text{ for } \beta^+ \text{ decay} \end{cases} \tag{3.14}$$

where $\alpha = e^2/\hbar c \simeq \frac{1}{137}$ is the fine-structure constant and $|Z|$ is the nuclear charge of the *decay product*.

For *negatrons* at the low-energy end of the spectrum, $\beta \ll 1$, and $F_N(Z,\eta) \to 2\pi y \propto \frac{1}{\eta}$. When the statistical factor $\eta^2(E_0 - E)^2\,d\eta$ is multiplied by $F_N(Z,\eta)$, the resulting momentum distribution of low-energy negatrons is approximately linear with momentum η, as shown by the curve marked β^- in Fig. 3.1, and also by the Cu^{64} β^- spectrum in Fig. 1.3.

For *positrons* at the low-energy end of the spectrum, $F_N(Z,\eta) \to 2\pi|y|e^{-2\pi|y|}$. Thus there is a very severe exponential reduction in the number of very-low-energy positrons in β^+ spectra. At first sight, it may be surprising that the coulomb effect hampers β^+ emission in comparison with β^- emission. The effect is not classical. Quantum-mechanically, there is a mutual potential barrier between the positron and the positively charged nucleus. In order to be emitted, the positron must penetrate this potential barrier. We see that for low-energy positrons $F_N(Z,\eta)$ contains the typical barrier transmission factor $e^{-2\pi|Z|/137\beta}$, in close analogy with the Gamow factor for α rays. The effect on the momentum distribution is shown by the curve marked β^+ in Fig. 3.1.

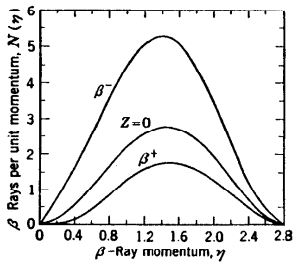

Fig. 3.1 Nuclear coulomb effects on the momentum distribution in allowed β-ray spectra. The curve marked $Z = 0$ contains only the effect of the statistical factor. The other two curves show the modifications of this spectrum ($\eta_0 = 2.8$; $E_{max} = 1.0$ Mev) produced by the nuclear coulomb factor, as evaluated (N5) for negatron or positron decay of calcium ($Z = 20$). Note the enhancement of the β^--decay probability in all portions of the spectrum. Conversely, the coulomb barrier against positron emission suppresses the entire β^+ spectrum and nearly eliminates the emission of low-momentum positrons. All curves are drawn, using Eq. (3.17), for constant $|P|^2$. Coulomb effects on the energy-distribution curves are even more dramatic, because of the velocity factor $dW = \beta\,d\eta$. Compare, for example, Figs. 1.4 and 1.6.

Most of the nuclear coulomb effect is produced in the region within the K shell of atomic electrons. When the binding energy

$$B_K \simeq \left(\frac{Z}{137}\right)^2\left(\frac{m_0c^2}{2}\right)$$

of a K electron in the decay product is not $\ll m_0c^2$, a relativistic form for the coulomb factor should be used. This can be developed in terms of Dirac's electron theory, with the electron wave functions evaluated at the surface of the nucleus R, in order to avoid a singularity which occurs at the origin. To an excellent approximation, the relativistic nuclear coulomb factor (F31, K37) is

$$F(Z,\eta) = \left\{\frac{4(1+s/2)}{|\Gamma(3+2s)|^2}\left(\frac{2R}{\hbar/m_0c}\right)^{2s}\right\}\{\eta^{2s}e^{\pi\nu}|\Gamma(1+s+i\eta)|^2\} \quad (3.15)$$

where

$$s = [1-(Z/137)^2]^{\frac{1}{2}} - 1 \simeq -\frac{1}{2}\left(\frac{Z}{137}\right)^2 \quad (3.16)$$

is the negative of the K-shell binding energy, in m_0c^2 units; R is the nuclear radius; and $\hbar/m_0c = 386 \times 10^{-13}$ cm is the rationalized Compton wavelength of an electron. The coulomb parameter η remains as given in Eq. (3.14). In Eq. (3.15) the expression in the first curly braces depends on Z only, while that in the second curly braces is a complicated function of both Z and η. The entire expression reduces to $F(Z,\eta) \to F_N(Z,\eta) \to 1$, for $Z \to 0$.

For a number of years the application of Eq. (3.15) to many β spectra was hampered by the inadequacy of existing tables of the complex Γ function. This has been remedied by the publication in 1952 of "Tables for the Analysis of Beta Spectra," from the National Bureau of Standards (N5), where the expression in the second curly braces of Eq. (3.15), after multiplication by η^2, is called $f(Z,\eta)$ and is tabulated over a wide range of η and for $Z = 1$ to 100. A numerical comparison of these values with those given by several analytical approximations which were used in β-ray spectroscopy prior to 1952 has been given by Feister (F24). The nonrelativistic approximation [Eq. (3.13)] has less than 5 per cent error for $Z \leq 30$, and $0.6 \leq \eta \leq 5$.

Screening by Atomic Electrons. In addition to the nuclear coulomb effect $F(Z,\eta)$, the electrostatic potential of the atomic electrons affects the shape of β-ray spectra. These corrections cannot be expressed in a simple analytical form. Reitz (R14) has tabulated the corrections due to "outer screening," for β^- and β^+ rays from 1.5 kev to 400 kev, in the elements $_{16}$S, $_{29}$Cu, $_{49}$In, $_{84}$Po, and $_{92}$U. The required solutions for the relativistic motion of a Dirac electron in the field of a Thomas-Fermi atom were obtained by electronic integration on the ENIAC computer. As was expected from previous approximate calculations of the screening correction by Rose and by Longmire and Brown, the atomic electrons exert very little influence on negatron β^- spectra but may profoundly affect the low-energy end of positron β^+ spectra, especially in heavy elements.

Screening by atomic electrons *reduces* the probability of β^- emission by about 2 per cent for a 50-kev β^- ray at $Z \sim 50$, and the effect is enhanced as Z increases or as the β^--ray energy decreases. For positron emission, the effects of screening by atomic electrons are much more important, because the potential of the atomic electrons has the effect of reducing the height and thickness of the potential barrier which must be penetrated by the emitted positron. Screening therefore tends to *increase* the probability of positron emission, while reducing the probability of negatron emission. For a 50-kev positron β^+ ray, the probability of emission is increased by about 37 per cent at $Z \sim 50$ and by a factor of 2.9 at $Z \sim 92$.

In general, electron screening can be thought of as having only a small suppressive effect on the low-energy end of β^- spectra, but of enhancing considerably the emission of low-energy β^+ rays, especially below, say, 100 kev in the heavier elements.

Allowed Spectra, β^+/β^- Ratio. We can now substitute analytical expressions into Eq. (3.3) in order to obtain a general formulation of the probability $N(\eta)\,d\eta$ for the emission of a β ray whose momentum lies between η and $\eta + d\eta$, when the nuclear disintegration energy is $W_0 = (E_{max}/m_0c^2) + 1$ and screening by the atomic electrons is neglected. This final expression for the shape of an allowed β-ray spectrum is

$$N(\eta)\,d\eta = \left(\frac{64\pi^4 m_0^5 c^4 g^2}{h^7}\right)|P|^2\,F(Z,\eta)\eta^2(W_0 - W)^2\,d\eta \quad (3.17)$$

where the nuclear coulomb factor $F(Z,\eta)$ is given by Eq. (3.15).

Experimental tests of Eq. (3.17) have been made, using a variety of radionuclides. A nearly ideal case is Cu^{64}

$$\begin{array}{ll} & \beta^- + {}_{30}Zn^{64} \qquad E_{max} = 0.57 \text{ Mev} \\ {}_{29}Cu^{64} & \\ & \beta^+ + {}_{28}Ni^{64} \qquad E_{max} = 0.66 \text{ Mev} \end{array} \quad (3.18)$$

which emits allowed β^- and β^+ spectra, of comparable energy, and comparable intensity ($\beta^-/\beta^+ \simeq 2.0$). Instrumental effects due to the scattering of low-energy β rays in sources of finite thickness, as well as changes of detector efficiency with β-ray energy, therefore tend to be nearly equal in the two spectra. A sensitive test of the Fermi theory is obtained by comparing the number of positron and negatron β rays in the *same* momentum interval η to $\eta + d\eta$. From Eq. (3.17), the ratio of positrons $N_+(\eta)$ to negatrons $N_-(\eta)$ should be dominated by the "barrier" term $e^{\pi\nu}$ in $F(Z,\eta)$, while all other energy-dependent terms nearly cancel. Then

$$\frac{N_+(\eta)}{N_-(\eta)} = \frac{F_+(Z,\eta)}{F_-(Z,\eta)}\frac{|P|_+^2}{|P|_-^2}\frac{(W_0 - W)_+^2}{(W_0 - W)_-^2}$$
$$\simeq \text{const}\,\frac{e^{-\pi(Z-1)/137\beta}}{e^{\pi(Z+1)/137\beta}} = \text{const}\,e^{-2\pi Z/137\beta} \quad (3.19)$$

where $Z = 29$ is the atomic number of the common parent Cu.

Figure 3.2 shows the ratio of positron to negatron β rays N_+/N_-, for various values of η, as observed by Wu and Albert (W75) using a Cu^{64} source of only $\sim$0.1-mg/cm^2 thickness in a solenoidal magnetic

β-ray spectrometer. The slight variations between theory and experiment at energies below about 50 kev are possibly of instrumental origin. This excellent agreement with the Fermi theory for the detailed shape of β-ray spectra has been confirmed in spectral measurements on even thinner sources of Cu^{64} ($\sim\mu g/cm^2$) prepared in uniform thickness by thermal evaporation onto very thin Zapon or Al source mounts by Langer, Moffat, and Price (L7) and by Owen and Cook (O7).

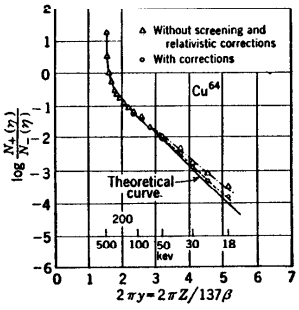

Fig. 3.2 Ratio of positrons to negatrons in the β spectra of Cu^{64}. The theoretical curve corresponds to Eq. (3.17), corrected for the effects of screening by atomic electrons. [*Adapted from Wu and Albert* (W75).]

Kurie Plot. Prior to the development of Fermi's theory, and the subsequent improvement of experimental techniques in β-ray spectroscopy (P18, C8), all efforts to deduce an analytical expression for the shape of β-ray spectra by empirical curve fitting were unsuccessful. However, with Eq. (3.17) in hand it is possible to devise coordinates such that allowed β-ray spectra may be plotted as straight-line graphs, as was first pointed out by Nordsieck and Kurie, Richardson, and Paxton (K50). For allowed transitions, the transition matrix element

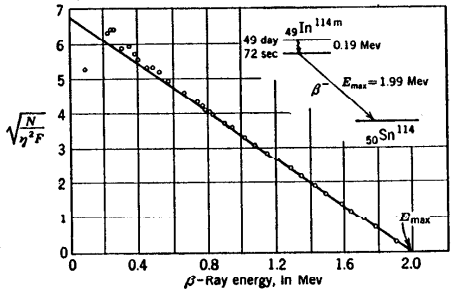

Fig. 3.3 Kurie plot of the β^- spectrum of In^{114}. Note especially that N means $N(\eta)$, the number of β rays in a *momentum* interval $\Delta\eta$ of constant size. The horizontal coordinate is the kinetic energy E which corresponds to the mid-point of the momentum interval η to $\eta + \Delta\eta$. When spectral data give a straight line, such as this one, then $N(\eta)$ is in agreement with the Fermi momentum distribution, Eq. (3.17). The intercept of this straight line, on the energy axis, gives the disintegration energy $E_{max}(= E_0)$, if the rest mass of the neutrino is zero. [*From Lawson and Cork* (L17).]

$|P|^2$ is independent of η. Then Eq. (3.17) can be put in the form

$$\left[\frac{N(\eta)}{\eta^2 F(Z,\eta)}\right]^{\frac{1}{2}} = \text{const}\ (W_0 - W) \tag{3.20}$$

Therefore a straight line results when the quantity $\sqrt{N/\eta^2 F}$ is plotted against a linear scale of β-ray energy, either as W or as E. Such graphs are called *Kurie plots*, or *Fermi plots*. They are especially useful for revealing deviations from the theory and for obtaining the upper energy limit, E_{max}, as the extrapolated intercept of $\sqrt{N/\eta^2 F}$ on the energy axis, at W_0 or E_0. Practically all new results on the shape of β-ray spectra are currently published as Kurie plots, rather than as actual momentum or energy spectra.

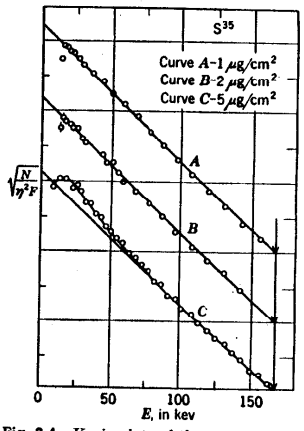

Fig. 3.4 Kurie plots of the β^- spectrum of S^{35}, showing improved agreement with the Fermi distribution as the source is made thinner and internal scattering is reduced. [*From Albert and Wu* (A11).]

As illustrations, Fig. 3.3 and Fig. 3.4 are Kurie plots for two historically important spectra, In^{114} and S^{35}. From 1935 until about 1939, the so-called Konopinski-Uhlenbeck, or K-U, modification (K40) of the Fermi theory was in vogue because it seemed to fit existing spectral data better than the original Fermi distribution. One predominant consequence of the Konopinski-Uhlenbeck theory (K40, K50, K37) was the replacement in Eq. (3.17) of $(W_0 - W)^2$ by $(W_0 - W)^4$. Kurie plots on the Konopinski-Uhlenbeck theory were therefore of $(N/\eta^2 F)^{\frac{1}{4}}$ against energy. As β-ray spectrometers and radioactive source preparation were improved, the apparent Konopinski-Uhlenbeck shapes were found to be instrumental distortions of Fermi shapes, brought about primarily by internal scattering of soft β rays in the source (T33, L15). The β^--ray spectrum of In^{114}, Fig. 3.3, provided conclusive evidence in favor of the Fermi distribution as given by Eq. (3.17). This radionuclide was well suited because, by good fortune, it combines a long half-period with a high-energy allowed β^- spectrum. It does this by virtue of a 49-day 0.19-Mev isomeric level, In^{114m}, which controls the decay rate and which decays to the 72-sec ground level of In^{114} from which an allowed β^- spectrum is emitted with $E_{max} = 1.99$ Mev. With such high-energy β rays, the effects of scattering in the source were minimized, and Lawson and Cork (L17) found a straight line Kurie plot of $\sqrt{N/\eta^2 F}$ against energy, as shown in Fig. 3.3.

Figure 3.4 shows Kurie plots for the β^- spectrum of S^{35}. This nuclide has a convenient half-period of 87 days but, as would be expected for a long-lived allowed transition, it emits only a soft β-ray spectrum, with $E_{max} = 0.167$ Mev. Albert and Wu (A11) found that deviations from a linear Kurie plot could be attributed to finite source thickness in the β-ray spectrometer. Figure 3.4 shows clearly that the Kurie plot becomes straight as the experimental technique is improved through the use of thinner sources.

Mass of the Neutrino. It will be qualitatively evident from Eqs. (3.4) and (3.7) that the shape of the β-ray spectrum depends on the rest mass m_ν assumed for the neutrino. The influence of a finite neutrino

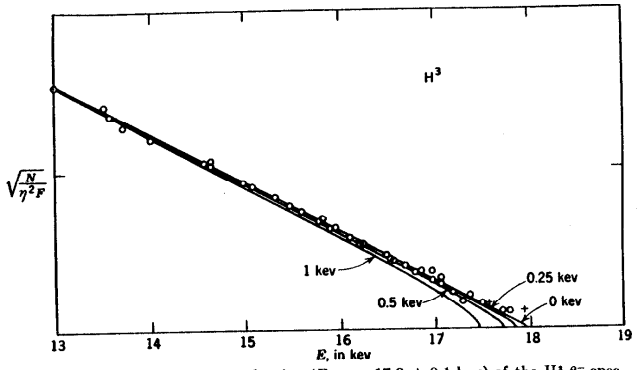

Fig. 3.5 Kurie plot near the end point ($E_{max} = 17.9 \pm 0.1$ kev) of the H^3 β^- spectrum. Theoretical curves which represent the effect of finite neutrino rest mass m_ν are drawn for $m_\nu = 0.25$ kev, 0.5 kev, and 1 kev. The data suggest that $m_\nu < m_0/2{,}000$. [*From Langer and Moffat* (L6).]

mass would be greatest near the upper energy limit E_0, where the Kurie plot would turn down sharply toward the energy axis, as shown in Fig. 3.5. It can be shown that this intercept should occur at an energy which is $m_\nu/2$ smaller than the extrapolated intercept of a straight-line Kurie plot, if the particle which accompanies β^- rays is a Dirac antineutrino. The corresponding energy difference is m_ν if the antineutrino and neutrino are identical ("Majorana neutrinos," Chap. 8, Sec. 3).

High-resolution measurements of the shape of the S^{35} spectrum (C38) and of the H^3 β^--ray spectrum (L6) near their end points have been made successfully with a large magnetic spectrometer. The experimental results for H^3, which are shown in Fig. 3.5, fix the rest mass of the Dirac antineutrino as less than 250 ev, or

$$m_\nu < \frac{m_0}{2{,}000} \tag{3.21}$$

where m_0 is the rest mass of an electron. A confirming result has been obtained in the case of H^3, using a spherical electrostatic integral spectrograph (H15). The assumption that the rest mass of neutrinos is identically zero is well supported by these experiments.

b. Shape of Forbidden β-Ray Spectra. The nuclear transition matrix element $|P|^2$ of Eq. (3.3) is independent of β-ray energy, in the case of allowed transitions, for any of the five theoretically possible forms of interaction between the transforming nucleon and the electron-neutrino field. All allowed transitions, on either Gamow-Teller or Fermi selection rules (Chap. 6, Sec. 3), have the spectral shape given by Eq. (3.17).

Konopinski and Uhlenbeck have calculated the shape factors which would apply to forbidden transitions on each of the five forms of interaction. The results are given in the form of shape correction factors C_n by which the allowed distribution of Eq. (3.17) must be multiplied (K37, K41, S47) in order to obtain the shape of the forbidden spectrum. The corresponding shape factor C_0 for allowed transitions is the constant $(1 + s/2)$ which appears in Eq. (3.15). It is found that many first-forbidden spectra and a few second-forbidden spectra (on a basis of log ft values) can and do have the same shape as allowed spectra. Well-established examples include Au^{198}, Re^{186}, and P^{32} (L8).

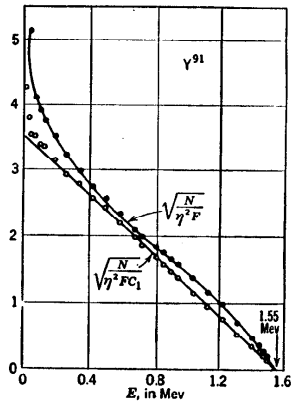

Fig. 3.6 Kurie plot of the Y^{91} first-forbidden ($\Delta I = 2$, yes) β spectrum. Solid points represent the ordinary Kurie plot of an allowed spectrum, Eq. (3.20). Open points, and a reasonably good fit, result when the first-forbidden shape correction factor C_1 of Eq. (3.22) is included. [*Adapted from Wu and Feldman* (W76, W73).]

The shape correction factor has a simple form for the parity-favored transitions, in which ΔI is one unit greater than the order of forbiddenness. For not too large Z, the theoretical correction factor for those Gamow-Teller first-forbidden transitions which have the selection rule $\Delta I = 2$, yes, is proportional to

$$C_1 \sim p^2 + q^2 \simeq (W^2 - 1) + (W_0 - W)^2 \tag{3.22}$$

where p and q are the momenta of the associated electron and neutrino. This shape factor provides for the emission of more high-energy β rays, and also more low-energy β rays if $W_0 > 2$ ($E_{max} > 0.51$ Mev), than are found in spectra which have the allowed shape.

Figure 3.6 shows the Kurie plot for the β^- spectrum of Y^{91} for which the shell model predicts (M27) a $p_{\frac{1}{2}} \rightarrow d_{\frac{5}{2}}$ transition, thus $\Delta I = 2$, yes. The ordinary Kurie plot of $\sqrt{N/\eta^2 F}$ shows that there is an excess of

low-energy β rays and also of high-energy β rays. Inclusion of the shape factor given by Eq. (3.22) produces a straight-line Kurie plot and therefore represents agreement between theory and experiment. A number of other radionuclides have been found to have the unique first-forbidden shape factor given by Eq. (3.22), including (W73, S37, L8) Cl^{38}, A^{41}, K^{42}, Br^{84}, Rb^{86}, Sr^{89}, Sr^{90}, Sr^{91}, Y^{90}, Y^{91}, Sb^{125}, and the 92 per cent low-energy branch in Cs^{137}. These are sometimes called "*α-type forbidden spectra.*"

For parity-favored second-forbidden transitions ($\Delta I = 3$, no), such as Be^{10}, the shape correction factor is

$$C_2 \simeq p^4 + \tfrac{10}{9}p^2q^2 + q^4 \tag{3.23}$$

while for parity-favored third-forbidden transitions ($\Delta I = 4$, yes), such as K^{40}, the shape correction factor becomes (K39, W74)

$$C_3 \simeq p^6 + 7p^2q^2(p^2 + q^2) + q^6 \tag{3.24}$$

Some second-forbidden ($\Delta I = 2$, no) transitions have been found to have shapes which are also relatively simple. Thus the 8 per cent high-energy branch in Cs^{137} has (L5) a shape factor which is well approximated by $C_{2T} \simeq (W_0 - W)^2 + 0.030(W^2 - 1)$.

Details of the rapid advance of knowledge concerning the shape and half-period of forbidden β spectra will be found in the excellent reviews by Wu (W73, W74) and by Konopinski and Langer (K39).

c. Half-period for β Decay. The probability of β decay per unit time, and into a momentum interval $d\eta$, is given by Eq. (3.17). The total probability of decay per unit time, which is the radioactive decay constant λ, is simply the integral over all possible values of η, that is,

$$\lambda = \frac{\ln 2}{T_{\frac{1}{2}}} = \int_0^{\eta_0} N(\eta)\, d\eta \tag{3.25}$$

where $T_{\frac{1}{2}}$ is the partial half-period for the particular mode of β decay involved.

The results of the integration in Eq. (3.25) are more generally useful if the momentum distribution is first transformed to the corresponding energy distribution. Making use of the relationships $W^2 = \eta^2 + 1$, $W\, dW = \eta\, d\eta$, and $F(Z,\eta) = F(Z,W)$, the energy distribution which is equivalent to Eq. (3.17) is

$$N(W)\, dW = \frac{|P|^2}{\tau_0} F(Z,W)(W^2 - 1)^{\frac{1}{2}}(W_0 - W)^2 W\, dW \tag{3.26}$$

where

$$\tau_0 \equiv \frac{h^7}{64\pi^4 m_0^5 c^4 g^2} \tag{3.27}$$

and $N(W)\, dW$ is the number of β particles in the energy range W to $W + dW$. The universal time constant τ_0 is a new natural constant, which has its origin in the Fermi constant, $g \sim 10^{-49}$ cm³ erg, but is easier to visualize because τ_0 is an ordinary time interval of the order of an hour. A closer experimental estimate of τ_0 will be made in Eq. (3.33). Then the partial decay constant λ and the associated partial half-period

$T_{\frac{1}{2}}$ can be written

$$\lambda = \frac{0.693}{T_{\frac{1}{2}}} = \int_1^{W_0} N(W)\, dW \equiv \frac{|P|^2}{\tau_0} f(Z,W_0) \tag{3.28}$$

The *Fermi integral function* $f(Z,W_0)$ can be evaluated analytically only for the limiting case of $Z = 0$, when the coulomb factor $F(Z,\eta) = 1$. Then

$$\begin{aligned} f(0,W_0) &= \int_1^{W_0} (W^2 - 1)^{\frac{1}{2}}(W_0 - W)^2 W\, dW \\ &= (W_0^2 - 1)^{\frac{1}{2}}\left(\frac{W_0^4}{30} - \frac{3W_0^2}{20} - \frac{2}{15}\right) \\ &\quad + \frac{W_0}{4}\ln\left[W_0 + (W_0^2 - 1)^{\frac{1}{2}}\right] \end{aligned} \tag{3.29}$$

The logarithmic term is important at low energies only. Expansion of Eq. (3.29) gives a useful approximation for small energies, which is

$$f(0,W_0) = 0.2155(W_0 - 1)^{\frac{1}{2}} + 0.0898(W_0 - 1)^{\frac{1}{2}} + \cdots \tag{3.30}$$

For intermediate values of W_0, $f(0,W_0)$ has the following values

W_0	1	1.2	1.4	2	3	4	5	6	8	11
$[f(0,W_0)]/W_0^5$	0	0.0003	0.002	0.0098	0.0196	0.0247	0.0274	0.0292	0.0310	0.0320

For large energies, a good approximation is

$$f(0,W_0) \simeq 0.030W_0^5 \tag{3.31}$$

This important result shows that, other factors being equal, the half-period for β decay follows the so-called "fifth-power law of β decay," that is, $T_{\frac{1}{2}} \propto (E_{max} + m_0c^2)^{-5}$. [It should be noted in passing that one reason for abandoning the Konopinski-Uhlenbeck modification (K40) of the Fermi theory was that it predicts a variation of $f(0,W_0)$ with W_0^7, in disagreement with experiment.]

Evaluation of $f(Z,W_0)$ for finite Z is laborious but has been carried out by graphical integration and with the use of approximate forms for the coulomb factor $F(Z,\eta)$. The results have been prepared as graphs of $\log_{10}[f(Z,W_0)]$ vs. W_0, for values of Z from 0 to ± 100 in steps of $\Delta Z = 10$, by Feenberg and Trigg (F22), and as graphs of

$$\frac{f(Z,W_0)}{f(0,W_0)}$$

by Moszkowski (M61). Representative values of $f(Z,W_0)$ are plotted in Fig. 3.7.

It will be noted that, for not too large Z/η, a reasonable rough approximation for $f(Z,W_0)$ can be obtained by representing the coulomb factor, Eq. (3.13) or Eq. (3.15), as $e^{\pi\bar{y}}$, where $\bar{y}$ is an average value of

$$y = \frac{\pm Z}{137\beta}$$

for the β spectrum. Then

$$f(Z,W_0) \simeq e^{\pi\bar{\nu}} f(0,W_0) \qquad \text{small } \frac{Z}{\eta} \tag{3.32}$$

Universal β-Ray Time Constant. The squared nuclear transition matrix element $|P|^2$ can be evaluated theoretically for only a few transitions (K39, K30, G17). Among these is the $\Delta I = 1$, no, transition ($^1S_0 \rightarrow {}^3S_1$)

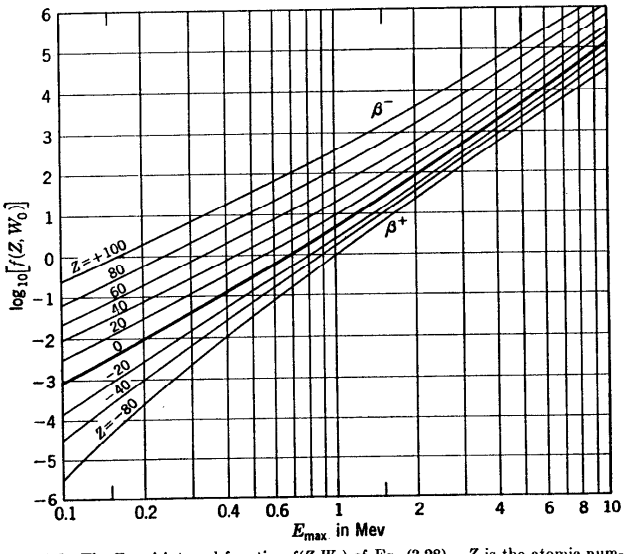

Fig. 3.7 The Fermi integral function $f(Z,W_0)$ of Eq. (3.28). Z is the atomic number of the *decay product* and is positive for negatron β^--ray emitters and negative for positron β^+-ray emitters. The nuclear disintegration energy $W_0 = [(E_{max}/m_0c^2) + 1]$ is expressed directly as E_{max} in Mev on the abscissas. The curve for $Z = 0$ is $f(0,W_0)$ of Eq. (3.29). [*Adapted from Feenberg and Trigg* (F22).]

of He^6, which is superallowed with $|P|^2 = 6$ on Gamow-Teller selection rules but would be forbidden on Fermi selection rules (Table 3.1, Chap. 6).

For He^6, $E_{max} = 3.50$ Mev, and $T_{\frac{1}{2}} = 0.823$ sec (H61). Then $W_0 = 7.86$, $f(3,W_0) \simeq 1{,}000$, and

$$\tau_0 = \frac{T_{\frac{1}{2}}}{0.693} |P|^2 f(Z,W_0) \simeq 7{,}000 \text{ sec} \tag{3.33}$$

Thus τ_0 is in the domain of 7,000 sec. From Eq. (3.27) the Fermi g constant becomes

$$g_{GT} \simeq 1.6 \times 10^{-49} \text{ cm}^3 \text{ erg} \tag{3.34a}$$

for β interactions which follow the Gamow-Teller selection rules (tensor or axial vector interaction).

In contrast with He^6, the β decay of O^{14} appears to follow Fermi selection rules in substantially all its transitions (G17). Within an experimental accuracy of $\sim$0.3 per cent, the positron β decay of O^{14} goes entirely to the excited level at 2.31 Mev in N^{14} (Fig. 4.1 of Chap. 11) which is known from other evidence to have $I = 0^+$. Thus the transition is $0^+ \rightarrow 0^+$, that is, $\Delta I = 0$, no, which is allowed on Fermi selection rules and forbidden on Gamow-Teller rules. The β-ray spectrum is found to have an allowed shape and an end point of 1.835 $\pm$ 0.008 Mev. For this transition, the Fermi matrix element has the theoretical value $|P|^2 = 2$. Combining these values with the half-period of 72.1 $\pm$0.4 sec, Gerhart (G17) finds for the Fermi g constant, in a pure Fermi transition,

$$g_F = 1.374 \pm 0.016 \times 10^{-49} \text{ cm}^3 \text{ erg} \tag{3.34b}$$

Within present experimental accuracy, it appears that $(g_{GT})/(g_F)$ is very close to unity. A number of β transitions may involve mixtures of Fermi and Gamow-Teller selection rules.

Comparative Half-period. As discussed in Chap. 6, the degree of forbiddenness of β-ray transitions can often be estimated from its so-called comparative half-period $ft \equiv [f(Z,W_0)]T_{\frac{1}{2}}$. From Eq. (3.28), the comparative half-period is

$$ft \equiv [f(Z,W_0)]T_{\frac{1}{2}} = \frac{0.693\tau_0}{|P|^2} = \frac{\text{universal constant}}{|P|^2} \tag{3.35}$$

For He^6, $ft \simeq 830$ sec, and for H^3, $ft \simeq 1{,}000$ sec. These are characteristic superallowed transitions, with $\log ft \sim 3$. Values of $\log ft$ for other transitions can be estimated readily from Eq. (3.35) and Fig. 3.7.

The comparative half-periods for forbidden transitions (Fig. 3.2 of Chap. 6) are usually evaluated using the value of $f(Z,W_0)$ which is characteristic of the shape of allowed spectra Eq. (3.28). When the shape of a forbidden spectrum has been evaluated, it is more appropriate to use a value of $f(Z,W_0)$ which actually corresponds to the spectral shape. The group of nuclides for which $\Delta I = 2$, yes, were first treated in this way by Shull and Feenberg (S37), who found that a good approximation for the Fermi function $f_1(Z,W_0)$ of these particular transitions is

$$f_1(Z,W_0) \simeq (W_0^2 - 1)[f(Z,W_0)] \tag{3.36}$$

When the comparative half-periods of these $\Delta I = 2$, yes, transitions are computed as $\log f_1 t = \log [(W_0^2 - 1)ft]$, a narrow range of values is found, in the domain of $\log [(W_0^2 - 1)ft] \simeq 10.0 \pm 0.5$. The parity-favored transitions $\Delta I = n + 1$, where n is the order of forbiddenness, whose spectral shapes are given by Eqs. (3.22) to (3.24), have been evaluated by Davidson (D7).

Competition with Neutron Emission. Delayed Neutron Emitters. That β decay is an extremely slow nuclear process is well illustrated by the existence of several so-called *delayed neutron emitters*, such as (S69)

$$_{35}\mathrm{Br}^{87}\ (T_{\frac{1}{2}} = 55.6\ \mathrm{sec})$$

and $_{53}\mathrm{I}^{137}$ ($T_{\frac{1}{2}} = 22$ sec), which occur among the products of uranium or thorium fission.

Figure 3.8 shows the principal transitions in the decay of Br^{87} and its immediate products. The stable isobar of mass number $A = 87$ is $_{38}\mathrm{Sr}^{87}_{49}$, whose directly measured nuclear angular momentum is $I = \frac{9}{2}$. From the shell model and comparative half-periods *ft*, as discussed in Chap. 6, the angular momentum and the state of the odd nucleon have been evaluated for each of the levels, as shown on Fig. 3.8.

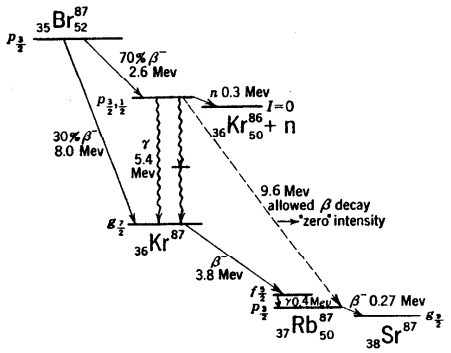

Fig. 3.8 Decay scheme of Br^{87} and its products. The 5.4-Mev excited level in Kr^{87} emits 5.4-Mev γ rays and 0.3-Mev neutrons, but the 9.6-Mev allowed β transition from this level to the ground level of Rb^{87} is too slow to be seen.

Some 70 per cent of the β transitions of Br^{87} go to the 5.4-Mev excited level in Kr^{87}. This is an allowed transition ($\log ft = 4.7$); hence the 5.4-Mev level is a $p_{\frac{3}{2}}$ or a $p_{\frac{1}{2}}$ state. It is the deexcitation of this 5.4-Mev level in Kr^{87} which interests us here.

The 5.4-Mev level in Kr^{87} lies about 0.3 Mev above the combined mass of Kr^{86} plus a neutron. Thus the neutron separation energy for Kr^{87} is $S_n \simeq 5.1$ Mev, and the 5.4-Mev level is a virtual, or unbound, level. Some two-seventieths of the excited Kr^{87} nuclei (or 2 per cent of the original Br^{87} nuclei) emit a neutron in the transition $\mathrm{Kr}^{87} \rightarrow n + \mathrm{Kr}^{86} + 0.3$ Mev. The mean life of the 5.4-Mev level is too short to be measured by present techniques, and $\frac{68}{70}$ of the time it decays by γ emission toward the ground level of Kr^{87}. The "delayed neutrons" are delayed entirely by the 55-sec half-period of their β-ray parent Br^{87}.

The 5.4-Mev level in Kr^{87} is 5.4 + 4.2 − 9.6 Mev above the $p_{\frac{1}{2}}$ ground level of Rb^{87}. An allowed β-ray transition ($\Delta I = 0$ or 1, no) could therefore take place with the release of 9.6 Mev. But even such an energetic β transition is much too slow to be seen in competition with deexcitation of the level by γ-ray emission and by neutron emission.

d. Electron-capture Transitions. Whenever it is energetically allowed by the mass difference between neighboring isobars (Chap. 3), a nucleus Z may capture one of its own atomic electrons, transforming to the isobar of atomic number $Z - 1$. Usually the electron-capture (EC) transition involves an electron from the K shell, because these have the greatest probability density of being in the nucleus. The L shell also contains two penetrating electrons, the so-called L_{I} s electrons with $l = 0$. The ratio of L_{I} capture to K capture is usually of the order of 10 per cent (R33), unless there is insufficient disintegration energy for K capture, when L_{I} capture takes place alone. We shall outline here only the theory of allowed EC transitions. The theory of forbidden transitions has been discussed by Marshak (M13), Bouchez (B103), and others.

In EC transitions, a nuclear proton changes to a neutron, and the disintegration energy is carried away by a neutrino; thus,

$$p + e^- \rightarrow n + \nu \tag{3.37}$$

The residual nucleus may be left in either its ground level or an excited level. The companion reaction, positron capture ($n + e^+ \rightarrow p + \bar{\nu}$), is not seen because it is impossible to produce a density of positrons at the nucleus which is comparable with the density of atomic electrons.

The fundamental difference between EC and its competing β^+ emission is that in EC transitions a *bound* electron is absorbed, rather than one from the continuum of negative energy states, in which a hole corresponds to positron emission. The total energy of a bound K electron can be written as

$$m_0c^2 - B_K \simeq m_0c^2(1 + s) = m_0c^2\sqrt{1 - \left(\frac{Z}{137}\right)^2}$$

where s is always negative and is defined as in Eq. (3.16). Then if the disintegration energy available for β^+ emission is $W_0 = (E_0/m_0c^2) + 1$, where as usual $E_0 \equiv E_{\max}$ of the β^+ spectrum, the disintegration energy available for EC is

$$W_0 + 1 + s \simeq W_0 + 1 = \frac{E_0}{m_0c^2} + 2 \tag{3.38}$$

Neglecting the kinetic energy of the recoil atom, Eq. (3.38) gives the kinetic energy of the emitted neutrino.

In contrast with Eq. (3.7), the phase-space volume is determined entirely by the energy of the emitted neutrino, because the electron is in a definite quantum state before its capture. In place of Eq. (3.12),

the statistical factor for EC is then simply

$$\frac{4\pi m_0^2 c}{h^3}(W_0 + 1 + s)^2 \tag{3.39}$$

The electron wave function ψ_e in Eq. (3.3) is to be replaced for EC transitions by the relativistic wave function of a bound K electron, and a factor of 2 introduced because either of the two K electrons can be captured. The calculation gives (K37, B68) for the probability λ_K of K capture per unit time

$$\lambda_K = \frac{|P|^2}{\tau_0} f_K \tag{3.40}$$

where the squared transition matrix element $|P|^2$ is the same as for the competing β^+ transition, τ_0 is the universal time constant of β decay [Eqs. (3.27) and (3.33)], and the function $f(Z,W_0)$ of β^+ decay is replaced for allowed K capture by

$$f_K = 2\pi\left(\frac{Z}{137}\right)^{3+2s}\left(\frac{2R}{\hbar/m_0c}\right)^{2s}\left[\frac{2+s}{\Gamma(3+2s)}\right](W_0 + 1 + s)^2 \tag{3.41}$$

$$f_K \simeq 2\pi\left(\frac{Z}{137}\right)^3 (W_0 + 1)^2 \tag{3.42}$$

where the symbols have the same meaning as in Eq. (3.15), except that for K capture Z is the atomic number of the *parent nucleus.*

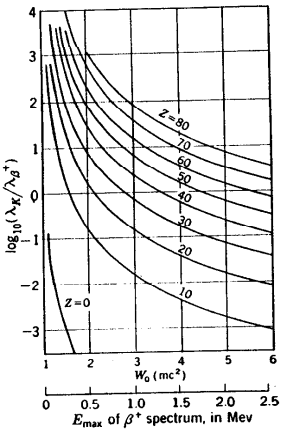

Fig. 3.9 Ratio of K-capture transition probability λ_K to positron β-ray transition probability λ_{β^+} for allowed transitions. Z is the atomic number of the *product nucleus,* as in the theory of β decay. Although positron emission is energetically excluded for $W_0 < 1$, K capture can take place in the energy domain $1 > W_0 > (-1 - s)$, where the ratio $\lambda_K/\lambda_{\beta^+} = \infty$. In terms of the masses of the initial and final atoms, $E_{max} = {}_{Z+1}M - {}_{Z}M - 2m_0c^2$ and $W_0 = [(E_{max}/m_0c^2) + 1]$. [*From Feenberg and Trigg* (F22).]

Ratio of Electron Capture to Positron β Decay. The same selection rules apply to EC transitions as to the competing β^+ transition. Then, in allowed transitions to any particular level of the residual nucleus, the ratio of the number of nuclei transforming by K capture to those transforming by β^+ emission is given by the ratio

$$\frac{\lambda_K}{\lambda_{\beta^+}} = \frac{f_K}{f(Z,W_0)} \simeq \frac{2\pi(Z/137)^3(W_0+1)^2}{f(Z,W_0)} \tag{3.43}$$

Measurements of the branching ratio between K capture and β^+ emission in a number of nuclei have been summarized by Bouchez (B103). Recalling that the experiments themselves are often quite difficult, the agreement with theory is good.

Figure 3.9 shows graphically how the ratio of K capture to positron β-ray emission depends on Z and the disintegration energy, for allowed transitions. Note that in heavy elements K capture is greatly favored over positron emission. For example, at $Z \sim 80$, a positron β-ray spectrum for which $E_{max} = 0.51$ Mev ($W_0 = 2$) will operate at a 1,000 to 1 disadvantage in comparison with K capture. The ratio of L_I capture to K capture also increases with Z and is about 0.15 for $Z \sim 80$ (R33). Thus, less than 0.1 per cent of the transitions will be by β^+ emission. This explains the complete absence of observable positron emitters among the heavy elements, which we noted in Chap. 16.

Physically, electron capture is favored in high-Z nuclides for two reasons. The electron orbits are smaller, and so there is a greater probability for an electron to be within the nuclear volume in heavy nuclei, and, secondly, the potential barrier $e^{-\pi|\eta|}$ of Eq. (3.15) against positron emission increases in effectiveness as Z increases.

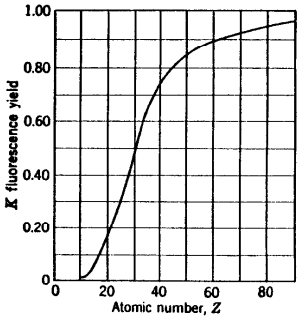

Fig. 3.10 Empirical variation of the K fluorescence yield with Z [*as compiled by Broyles, Thomas, and Haynes* (B135).]

Auger Electrons. Following K capture, there is an electron vacancy in the K shell. This is filled by a transition of an L electron into the K shell and the emission of either a K_α X-ray photon (especially in heavy elements) or an Auger electron (especially in light elements). The energy of the K_α photon is $(B_K - B_L)$; that of the competing L-shell Auger electron is $(B_K - 2B_L)$. B_K and B_L are the electron binding energies in the K and L shells of the product nucleus. The X-ray and Auger-electron spectra have been measured directly for a number of electron-capture nuclides (B135).

The competition between the emission of a K X ray and the emission of an Auger electron is described by the *K fluorescence yield,* which is defined as the number of K X-ray quanta emitted per vacancy in the K shell. The probability that a K X ray will be emitted is nearly unity in high-Z elements and nearly zero in low-Z elements. Figure 3.10 shows the empirical variation of this probability with Z (B135, B142).

Effect of Chemical Combination on Electron Capture. The density of L_I electrons at the position of the ${}_4Be^7$ nucleus will depend slightly on the chemical form of the beryllium. The possibility of producing by chemical means a change in the half-period of Be^7, which decays only by electron capture, was first demonstrated by Segrè and by Daudel. The effects are very small but definite. For comparison with the experimental

results, no adequate theory of the expected changes in electron density exists. The experimental results have been summarized and extended by Kraushaar, Wilson, and Bainbridge (K46), who find that the decay constant λ of metallic Be^7 is reduced by (0.013 ± 0.005) per cent when the Be^7 is in the form of BeO, and by an additional (0.061 ± 0.005) per cent when the Be^7 is in the form of BeF_2.

Problems

1. Calculate and plot the energy distribution spectra which correspond to the β-ray momentum spectra given in Fig. 3.1.

2. (*a*) Calculate the shape of the β-ray spectrum expected in the disintegration of the free neutron. Present the results as a momentum spectrum and a Kurie plot.

(*b*) If $|P|^2 = 3$ for an $s_{\frac{1}{2}} \rightarrow s_{\frac{1}{2}}$ transition on Gamow-Teller selection rules, calculate the expected half-period of the free neutron against β decay.

3. If the β transition $H^3 \rightarrow He^3 + \beta^-$ is regarded as allowed and corresponding to an $s_{\frac{1}{2}} \rightarrow s_{\frac{1}{2}}$ transition with $|P|^2 = 3$, calculate the expected half-period of H^3 if the maximum energy of the β-ray spectrum is 0.018 Mev and $\tau_0 \simeq 7{,}000$ sec.

4. The following series of mirror nuclides are all positron emitters, and none emits γ rays.

Nuclide.....	$_6C^{11}$	$_8O^{15}$	$_{10}Ne^{19}$	$_{12}Mg^{23}$	$_{14}Si^{27}$	$_{16}S^{31}$	$_{18}A^{35}$
β^+ E_{max}, Mev...	0.99	1.68	2.18	2.99	3.48	3.9	4.4
Half-period, sec..	1,230	118	18.2	11.9	4.9	3.2	1.88

(*a*) Calculate the *ft* values, and also the matrix elements for these transitions, using the approximation $f(Z,W_0) = e^{\pi\beta}f(0,W_0)$.

(*b*) Why would you expect the matrix elements for these transitions to be so similar?

5. N^{17} decays by β^- to an excited level of O^{17} with a maximum energy of 3.72 Mev. This excited level dissociates by neutron emission. F^{17} decays by positron emission with a maximum energy of 1.72 Mev. No γ rays are present in F^{17} decay. From other experiments the following values are known:

$$(n - H^1) = 0.78 \text{ Mev}$$
$$(N^{17} - O^{17}) = 8.80 \text{ Mev}$$
$$(O^{16}H^1 - F^{17}) = 0.59 \text{ Mev}$$

The known excited levels of O^{16} have excitation energies of 6.05, 6.13, 6.9, 7.1, and higher Mev.

(*a*) Using only the above data calculate the energy of the emitted neutrons in the laboratory system.

(*b*) Show all energies involved on an energy-level diagram for mass number 17.

CHAPTER 18

Ionization of Matter by Charged Particles

In the experimental study of the energy levels and transitions of nuclei, there are many cases which require the measurement of the kinetic energy of a swift charged particle by methods which depend upon absorption and scattering phenomena. Additionally, the response characteristics of every type of radiation-detection instrument depend upon the interaction of charged particles with the sensitive elements of the detector. In order to perform measurements, and to interpret them correctly, it is of fundamental importance to understand the various types of interaction between swift charged particles and matter. The term "swift particles," as used here, refers to particles whose velocities are very much higher than the velocities of thermal agitation.

The interactions which we shall consider here are those which are due primarily to *coulomb forces*. These include ionization, scattering, and various types of radiative losses. Interactions which involve the specifically nuclear short-range forces between nucleons have been discussed in detail in Chaps. 10 and 14.

In the following chapters we shall examine each mode of interaction, on a generalized basis, for swift particles of any mass and charge. Each of these general relationships will then be particularized for the case of "light" particles (electrons) and "heavy" particles (mesons, protons, α rays, . . .).

a. Interactions between Swift Charged Particles and Matter. The mechanisms by which a charged particle loses its kinetic energy, or is deflected from its original path, involve four principal types of interaction. These may be classified as follows:

1. *Inelastic Collision with Atomic Electrons.* Inelastic collisions with bound atomic electrons are usually the predominant mechanism by which a swift charged particle loses kinetic energy in an absorber. As a result of each such collision, one or more atomic electrons experience a transition to an excited state (excitation) or to an unbound state (ionization). These collisions are discussed in this chapter from the standpoint of energy transfer. The deflections experienced by the incident particle are treated in Chap. 19.

2. *Inelastic Collision with a Nucleus.* In a close, noncapture encounter with a nucleus, the incident charged particle invariably experiences a